ACSNANO

www.acsnano.org

ARTICLE

Broadband Near-Infrared to Visible Upconversion in Quantum Dot–Quantum Well Heterostructures

Ayelet Teitelboim and Dan Oron*

Department of Physics of Complex Systems, Weizmann Institute of Science, Rehovot, Israel 7610001

Supporting Information

ABSTRACT: **Upconversion is a nonlinear process in which two, or more, long wavelength photons are converted to a shorter wavelength photon. It holds great promise for bioimaging, enabling spatially resolved imaging in a scattering specimen and for photovoltaic devices as a means to surpass the Shockley–Queisser efficiency limit. Here, we present dual near-infrared and visible emitting PbSe/CdSe/CdS nanocrystals able to upconvert a broad range of NIR wavelengths to visible emission at room temperature. The synthesis is a three-step process, which enables versatility and tunability of both the visible emission color and the NIR absorption edge. Using this method, one can achieve a range of desired upconverted emission peak positions with a suitable NIR band gap.**

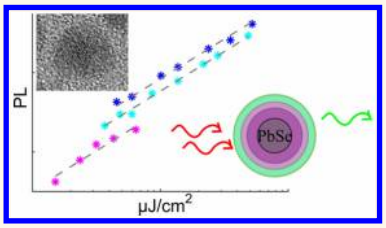

KEYWORDS: *semiconductor nanocrystals, upconversion, quantum dot-quantum well, near-infrared, intraband absorption, interband absorption*

Semiconductor nanocrystals (NCs) exhibit unique properties that differ from their bulk analogs due to quantum confinement effects. Studies involving these systems have recently advanced greatly in synthetic capabilities, enabling the fabrication of complex heterostructures composed of several materials. Such advances have led in recent years to the ability to fabricate nanoscale colloidal quantum dot–quantum well (QD-QW) systems. By tailoring the band alignment in a nanoparticle formed from concentric shells of varying materials, it is possible to obtain particles with two spatial regions that can confine carriers, both in the core and in an external shell. Formation of such coupled quantum dot–quantum well within a single colloidal nanoparticle has been demonstrated,[1] as well as architectures that enable control over the degree of coupling.[2] The latter results in heterostructures that exhibit two distinct spectral emission bands. The possibility to tune the optical and electronic coupling of the QD and the QW components arises from the ability to alter the barrier layer between the two quantum systems via control of both the spatial dimension and the relative band alignment.[3−6] Dual color emission originating from multiexciton emission was demonstrated in giant core–shell quantum dots (QDs),[7,8] and in core–shell tetrapods,[9−11] through suppression of auger recombination promoting emission of multiple photons having different wavelengths. Another approach for fabrication of dual-emitting semiconducting double quantum dots utilized tip growth in seeded nanorods.[12] Such systems have been shown to exhibit antibunching of the two emission colors as well as charge transfer between the two dots. One outcome of the ability to transfer charges from one dot to the other in such a structure is the achievement of incoherent luminescence upconversion (UC) in such a system.[13] UC is a nonlinear process in which two, or more, long wavelength (low energy) photons are converted to a shorter wavelength (high energy) photon.[14,15] This process is based on sequential absorption of two or more photons, involving metastable, long-lived intermediate energy states. It is markedly different from sum frequency generation (SFG) that is restricted to upconversion of coherent laser radiation as a coherent process. This sequential absorption leads to a population of highly excited states from which UC emission can occur. Hence, requirements for UC processes are long-lived excited states, a ladder-like arrangement of energy levels and a mechanism inhibiting cooling of the hot charge carrier.[16] The ability to upconvert low energy photons into a higher energy photon holds a significant promise and importance for many applications in different fields, such as imaging and photovoltaics. In imaging, UC enables spatially resolved imaging in a scattering specimen with almost no autofluorescence and high signal-to-noise ratio. This is analogous to two-photon excitation fluorescence but can be achieved at much lower excitation fluence, dramatically reducing photo damage by the excitation beam.[17] For photovoltaic devices, UC could be used to surpass the well-known Shockley–Queisser efficiency limit.[18] UC enables harvesting of photons with energies below the band gap by converting multiple photons to one photon that fits the

Received: August 25, 2015
Accepted: November 22, 2015

DOI: 10.1021/acsnano.5b05329
ACS Nano XXXX, XXX, XXX–XXX

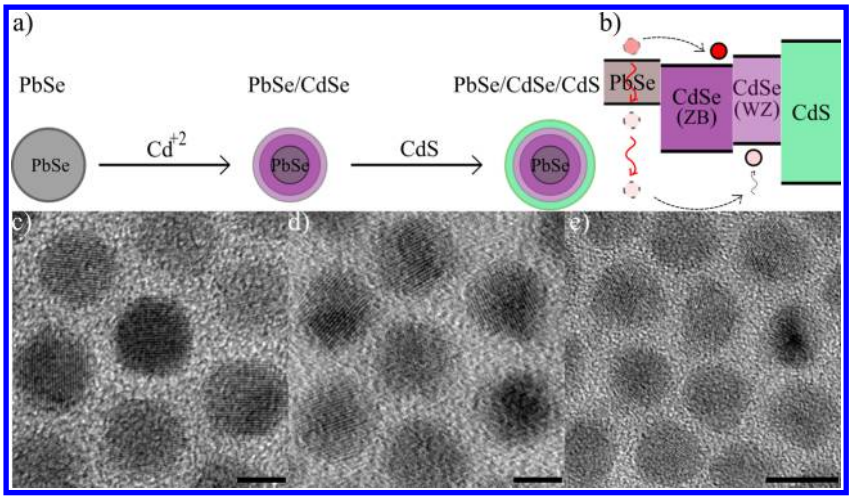

Figure 1. PbSe/CdSe/CdS synthesis and band alignment. (a) Three step synthesis scheme: core growth, cation exchange, and SILAR. (b) Schematic band alignment of PbSe/CdSe/CdS. (c)−(e) TEM images of S1 sample after each synthesis step depicted in (a) correspondingly. The scale bar represents 5 nm for images c and d and 10 nm for image e.

junction's bang gap. The inability to utilize these low energy photons in photovoltaic devices is a main loss mechanism.

However, efficient UC at room temperature is generally very difficult to achieve at low illumination intensities. The most common UC system implemented today is realized in solid materials (hosts) doped with ions of d and f elements (transition metals and rare earths), which possess a variety of metastable states.[19] Despite recent progress, such as using dopant blends,[20] and hybrid organic−inorganic systems,[21] these systems still suffer from low color tunability and relatively low absorption cross sections. Another method, which has achieved very high UC efficiency is triplet−triplet annihilation (TTA),[22−25] where two molecules excited to a long-lived triplet state, each by intersystem crossing from a singlet excited state, transfer their excitation energy to a higher energy singlet emitting state of a third molecule. However, as it relies on organic absorbers, this system suffers from a limited availability of near-infrared fluorophores, photobleaching, and restrictions forced by diffusion limits.

To quantify the efficiency of the UC process, we follow the definitions of ref 26, where the UC quantum yield is defined as the number of high energy photons emitted divided by the number of lower energy photons absorbed. Thus, the maximal UC efficiency obtainable is 50%, as it requires photon pairs. Because UC is a nonlinear process, the UC efficiency depends on the details of the excitation process, and particularly the excitation power density. The dependence of the UC efficiency on the excitation power density is quadratic at low powers and saturates at high excitation powers. It is thus reasonable to quote values for the UC efficiency at the rolloff point, where the quadratic power dependence is no longer obeyed. For upconversion QDs,[13] this occurs approximately when an average of one exciton per dot is excited in the ensemble. Bulk rare-earth-based UC materials have reached efficiencies of up to about 5%,[26] whereas TTA in solution has been shown to achieve higher efficiencies, up to a few tens of percent. Both rare-earth-based systems and TTA based ones have already been used in nanocrystalline form. Yet, UC nanocrystals typically achieve much lower efficiency, of the order of 1%.

Semiconducting NCs hold a great promise for UC, benefiting from high tunability, easily achieved by the quantum confinement effect, combined with high stability and low photobleaching. Deutsch et al.[13] presented a system of upconverting NCs, which incorporates two quantum dots with different bandgaps separated by a tunneling barrier. This system was able to upconvert 680 nm into 570 nm light. It was shown that these NCs can operate at room temperature, with the dominant mechanism proven to be sequential interband and intraband absorption events.

In this work heterostructure NCs that are able to upconvert near-infrared (NIR) light at wavelengths up to about 1.2 μm to visible light, implying a relatively small energy loss ($2E_{IR} - E_{Vis}$) during the process, are presented. Realizing a system that will be able to upconvert NIR photons to higher energy visible photons using NCs requires not only coupling of a NIR absorber to a visible light emitter but also a proper band alignment between the two, such that hot excitons resulting from the absorption of two NIR photons will be efficiently harvested. For this end, a double well band alignment is required for one charge carrier (electrons or holes), where the barrier has to be sufficiently thick to prevent tunneling from the higher energy well to the lower energy one. In contrast, the other type of the charge carriers should be delocalized across the particle through its degenerate band. This type of structure is schematically depicted in Figure 1.

RESULTS AND DISCUSSION

To experimentally realize this system in a tunable and versatile manner, we chose the PbSe/CdSe(ZB)/CdSe(WZ) core/shell/shell system. Recently, it was shown that small PbSe cores with a thick CdSe shell exhibit double emission as a result of slow cooling of holes from the CdSe shell to the PbSe core.[27,28] The existence of double emission hints that these particles exhibit a double well potential needed for UC. Indeed, a recent study on giant PbS/CdS core−shell QDs indicated that the large volume shell of the CdS is composed partly of zinc blende (ZB) CdS and partly of Wurzite (WZ) CdS.[29] In these particles the WZ phase grew over the ZB with a crystallographic orientation leading to highly asymmetric tetrahedral QDs. Keeping in mind that ZB and WZ have a band offset[30,31] that may result in the formation of an energetic barrier in the valence band between the PbS and the CdS wells, it is suggested that the visible emission originates from the WZ outer shell. It is therefore

DOI: 10.1021/acsnano.5b05329
ACS Nano XXXX, XXX, XXX−XXX

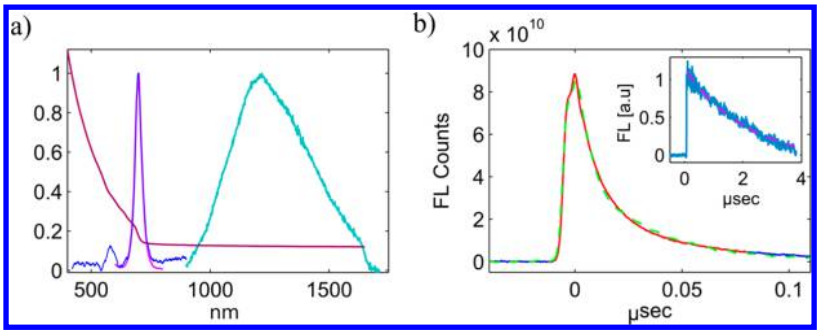

Figure 2. S1 PbSe/CdSe/CdS optical characteristics. (a) Linear emission spectrum, using a 405 nm LED excitation, the visible emission and the NIR emission of sample S1 are depicted in blue and cyan correspondingly (The calibrated photon emission spectra show a ratio of 1.7 between the total number of NIR and visible photons). In pink is the UC spectrum, corresponding to the integrated transient limits shown in (b). The absorption spectrum is depicted in maroon and is vertically shifted for clarity. A zoom-in on the NIR absorption is provided in the Supporting Information. (b) Typical UC transient curve of the visible emission peak at 700 nm, using 850 nm excitation at 52 mJ/cm^2, is depicted in blue. The integrated area for UC spectrum counts calculation for each wavelength is depicted in red. The transient response is well fitted by a biexponential decay having an average lifetime of 6.3 ± 0.2 ns when convolved with the 8 ns instrument response function (dashed green) The PbSe NIR emission lifetime, depicted in the inset, is well fitted by a single exponential of 2.1 ± 0.1 μs.

likely that a similar mechanism is at play also for PbSe/CdSe heterostructures.

Although the band gap of the NIR-absorbing PbSe core can be easily tuned by its size, its quasi type II band alignment with CdSe makes it suitable for upconversion via hot hole injection to CdSe. As can be seen in the band alignment scheme in Figure 1b, PbSe and CdSe have a relatively flat conduction band (CB), enabling the electron to delocalize throughout the NCs. However, because PbSe is a low band gap material, the valence band (VB) is relatively deep, creating a spatially separate two-well potential VB. As depicted in Figure 1b, hot holes can reach the wurtzite CdSe VB, where they can recombine with electrons creating higher energy photons. In the following we thus test the ability of such particles to act as UC nanocrystals for the NIR spectral range.

For this purpose, relatively large, 7.6 nm diameter, PbSe core QDs were synthesized. Partial cation exchange from PbSe to CdSe was used to blue shift the PbSe NIR PL to around 1230 nm while creating the PbSe/CdSe interface needed for upconversion. A CdS shell was added on top of the CdSe shell for surface passivation by using successive ion absorption and reaction (SILAR).[32] The addition of this layer ensures stability and increases the quantum efficiency of the CdSe emission. This system will hereafter be denoted as "S1". The different stages of the PbSe/CdSe/CdS synthesis are depicted in Figure 1, with TEM images corresponding to each of the steps. As can be seen in Figure 1d, the PbSe QDs maintain their original size and shape after cation change, shifting the NIR fluorescence to about 1230 nm gradually (Figure 2). After completing only one atomic layer of CdS shell, a strong visible second florescence peak around 700 nm is observed, while the NIR emission spectrum remains relatively unchanged (see Figure 2a for the NIR and visible fluorescence spectra). More detailed synthesis procedures are described in the Supporting Information. After SILAR the NCs receive a slight pyramidal shape.

Detailed characterization and optical studies of the upconversion process were made on sample S1. Transient visible emission spectra were taken in each measurement around the fluorescence peak at 700 nm for a series of increasing excitation power densities to extract the power dependence of the upconverted emission. Details of the optical setup used in these measurements appear in the Supporting Information. Taking a power series was necessary to distinguish between the nonlinear upconversion process, which requires two photon excitation and possible alternative mechanisms. In the case of excitation above the band gap of CdSe, which is energetic enough to directly excite the CdSe (WZ) with only one photon, the power dependence should be linear. Thus, 480 nm excitation was used here as reference for linear excitation. For a NIR excitation the power dependence should be quadratic, as it is absorbed only by the PbSe core and requires two-photon UC to reach the CdSe (WZ) well.

As an example of one such measurement, the properties of upconverted luminescence using a 52 mJ/cm^2 850 nm excitation are shown in Figure 2. Figure 2b presents the emission transient observed at the upconverted emission peak maximum (700 nm). The emission lifetime τ was assessed using a biexponenetial fit $A_1 \cdot e^{-(t/\tau_2)} + A_2 \cdot e^{-(t/\tau_1)} + c$ convolved with the instrument response function (where A is the exponent amplitude and c is an offset). A characteristic lifetime of 6.3 ± 0.2 ns decay was found for these particles, similar to that observed using visible excitation at 480 nm. Notably, the observed emission lifetime was independent of the NIR excitation wavelength (Figure SS4). As can be seen in Figure 2a, the upconverted emission spectrum using excitation at 850 nm agrees well with the emission spectrum as measured using linear excitation with a 405 nm LED, depicted in magenta and blue correspondingly. These findings clearly indicate that upconverted hot excitons, which reach the CdSe (WZ) have similar photophysics as excitons directly generated in the CdSe (WZ) by excitation in the visible (480 nm). This agreement reassures that indeed the UC signal originates from hot charge injection from the PbSe core to the CdSe shell, and that a CdSe (ZB) barrier exists.

A second important feature of the upconversion process is depicted in Figure 3 which shows the power dependence ($P_{ex}(w_{2ph})$) of fluorescence at the spectrum peak at 700 nm, for a variety of NIR excitation wavelengths (w_{2ph}): 850, 900, 950, 1050, and 1100 nm. As expected for a 2-photon process, each of the different power dependent excitations graphs fits a quadratic power law $a(w_{2ph}) \cdot P_{ex}(w_{2ph})^2$, which is depicted by the dashed lines.

The amplitude for the quadratic dependence prefactor ($a(w_{2ph})$) for each excitation wavelength w_{2ph} can be plotted vs the corresponding absorbance of the NCs at this wavelength

DOI: 10.1021/acsnano.5b05329
ACS Nano XXXX, XXX, XXX−XXX

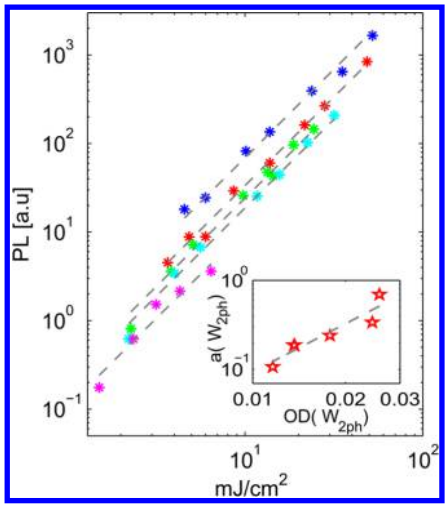

Figure 3. S1 PbSe/CdSe/CdS power dependent UC fluorescence counts of the visible emission peak at 700 nm, for a variety of NIR excitations at 850, 900, 950, 1050, and 1100 nm (depicted in blue, red, green, cyan, and magenta correspondingly). Each of the different power dependent excitations was fitted by a quadratic power law $a(w_{2ph})\cdot P_{ex}(w_{2ph})^2$, which is depicted by the dashed gray lines. The inset shows the amplitude of the quadratic dependence prefactor ($a(w_{2ph})$) for each excitation w_{2ph} vs the corresponding absorption of the NCs in this wavelength ($OD(w_{2ph})$). Fitting this using power distribution $a(w_{2ph}) = A\cdot OD(w_{2ph})^b$ reveals a power dependence (b) of 1.8 ± 0.96, depicted by the dashed gray line. The graphs are depicted on a log−log scale.

($OD(w_{2ph})$). This should show the dependence of the upconversion process on the particles' absorption cross section. We plot this in the inset of Figure 3, where each point in the plot corresponds to the 2ph excitation amplitude and absorption, for wavelengths (w_{2ph}) 850−1100 nm from right to left. Fitting this using power distribution $a(w_{2ph}) = A\cdot OD(w_{2ph})^b$ reveals a power dependence (b) of 1.8 ± 0.96.

UC in such NCs can originate from two possible mechanisms. The first is sequential interband absorption, leading to a biexciton, followed by Auger recombination generating a hot hole[33] (Figure 4a). The second is interband absorption followed by intraband absorption of the hole (Figure 4b). Because the Auger recombination mediated process requires the creation of two excitons via interband absorption, a quadratic dependence on the linear absorption cross section is expected below saturation. In contrast, for the process depicted in Figure 4b the dependence on the absorption cross section is possibly weaker. This is due to the fact that the second intraband absorption cross section may have a weaker dependence on the excitation wavelength, due to the high density of states of the intraband final transition. This can thus result in a lower than quadratic power dependence on the absorption cross section. From our measurements, the deviation from quadratic dependence is not sufficiently significant to preclude either mechanism. In fact, it is likely that both processes contribute to UC in these particles.

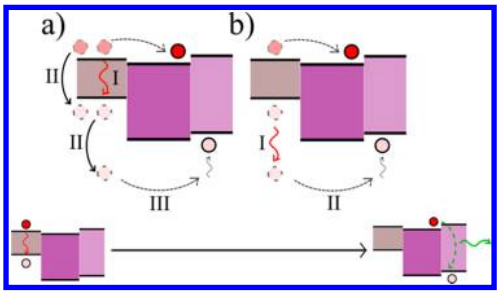

Figure 4. Two possible mechanisms that contribute to UC in PbSe/CdSe/CdS QDs. After the formation of an exciton via interband absorption, which is illustrated in the bottom left corner, a hot hole can be formed using the energy of a second photon. This can occur in two ways: (a) an Auger recombination mediated process, which requires the creation of two excitons, using a second photon via interband absorption, (b) an intraband absorption process. Both processes result in a hot hole which can transfer to the CdSe (WZ) well and relax by emitting a visible photon (bottom right corner).

Two important figures of merit of UC in NCs systems are the efficiency and the saturation intensity of the process. The saturation energy is an important parameter to consider, as pumping the system above this energy becomes less and less effective until high saturation where it will not contribute to an increase in fluorescence. In the case of these UC nanoparticles, saturation results in a linear power dependence rather than a quadratic one. To further extract the parameters of the system as an upconversion medium, saturation curves were made using a linear excitation at 480 nm and a 2ph UC excitation at 1064 nm. As can be seen in Figure 5a, and as expected for a 480 nm excitation that can excite directly the CdSe (WZ), this excitation results in a linear saturation. The excitation probability in QDs, using an excitation above the band gap, can be roughly modeled using a Poissonian distribution: $(n) = (\lambda^n/n!)e^{-\lambda}$. This distribution reflects the probability to excite n number of excitons using a distribution parameter $\lambda = (I/I_{sat})$, where I_{sat} is the saturation energy for these particular NCs. In the case of linear saturation, the probability to excite the QD at least once is given by $P(n \geq 1) = 1 - P(0) = (1 - e^{-(I/I_{sat})})$. Here, I_{sat} is the excitation value in which the emission is $1 - (1/e) \cong 0.6$ of its maximal value. This results in a saturation intensity of I_{sat} = 1.8 ± 0.7 mJ/cm^2. In contrast, as depicted in Figure 5b, the saturation curve for the UC process using a 1064 nm excitation does not show linear saturation, and indeed, it required the consideration of a 2ph process. To fit the UC saturation, the probability to absorb multiple photons for the UC process has to be accounted for. This is done by using the simplified Poissonian distribution for the probability to absorb photon pairs, resulting with

$$FL_{UC} = \left(\frac{\lambda^2}{2!} + 2\cdot\frac{\lambda^3}{3!} + 3\cdot\frac{\lambda^4}{4!} + 4\cdot\frac{\lambda^5}{5!} + 5\cdot\frac{\lambda^6}{6!} + \ldots\right)\cdot e^{-\lambda}\cdot \epsilon_{UC}$$

where $\epsilon_{UC} < 1$ is the probably to heat up a hole and for it to be caught by the visible well before cooling down; i.e., ϵ_{UC} is the UC efficiency. For a more detailed model see the Supporting Information. This model gives a saturation energy of 356 ± 5 mJ/cm^2 for UC.

To assess the UC efficiency, a comparison can be made between the number fluorescence counts at saturation intensity per absorbed photon using either linear or two-photon excitation $[(FL_{UC_{sat}}/(I_{sat_{1064}}\cdot OD_{1064}))/(FL_{Lin_{sat}}/(I_{sat_{480}}\cdot OD_{480}))]$. As both the UC and the linear fluorescence counts were measured at the same concentration, this ratio is the probability to excite the CdSe (WZ) well, i.e., the efficiency of the UC process (ϵ_{UC}). This gives a 0.075 ratio, which means that every 7 NIR photon pairs absorbed are equivalent to one

DOI: 10.1021/acsnano.5b05329
ACS Nano XXXX, XXX, XXX−XXX

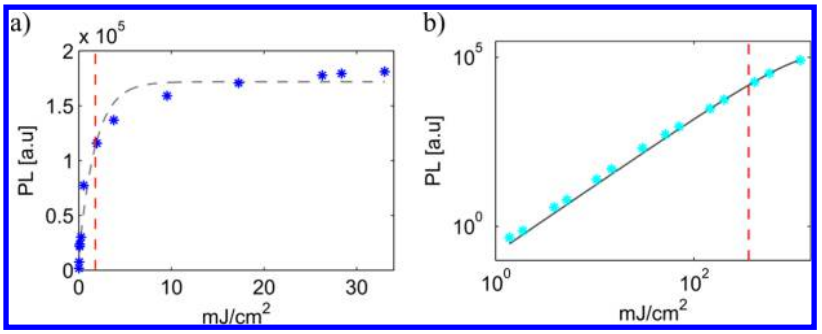

Figure 5. S1 PbSe/CdSe/CdS linear and 2ph UC saturations are depicted in (a) and (b), with a 480 and 1064 nm excitations correspondingly. The 2ph UC saturation is depicted on a log scale. The dashed gray line in (a) depicts the linear saturation fit, and the solid line in (b) depicts the 2-photon saturation fit. The linear fluorescence Poissonian fit model results in a saturation intensity of I_{sat} = 1.8 ± 0.7 mJ/cm^2, which is illustrated in a dashed red line in (a). The UC simplified Poissonian distribution gives a saturation energy of 356 ± 5 mJ/cm^2 which is illustrated in a dashed red line in (b).

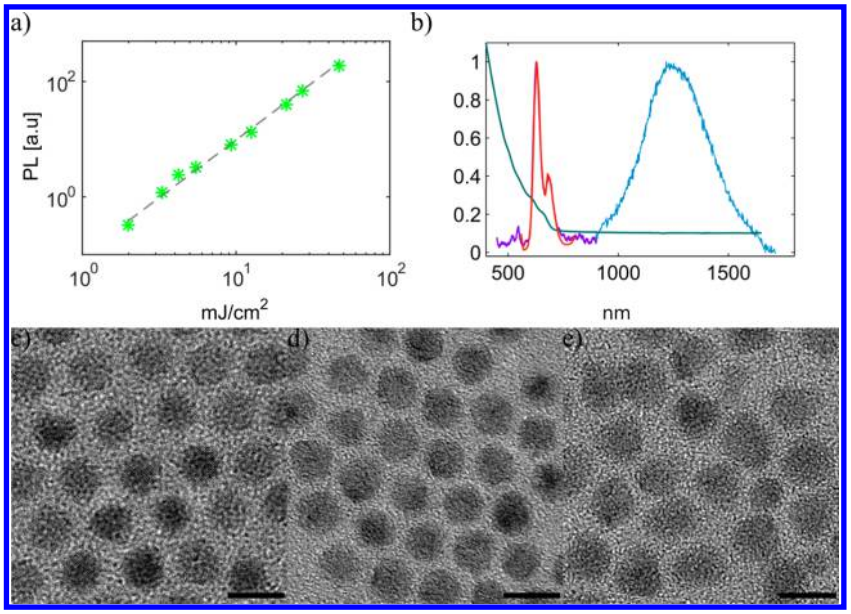

Figure 6. S2 PbSe/CdSe/CdS spectrum and power dependence. (a) S2 PbSe/CdSe/CdS power dependent UC fluorescence counts of the visible emission peak at 630 nm, for a 850 nm excitation, is depicted in green. The power dependent fit is depicted in dashed gray. (b) Linear emission spectrum, using a 405 LED excitation, for the visible emission and the NIR emission of sample S2 is depicted in purple and light blue correspondingly. In red, is the typical UC spectrum, corresponding to the integrated transient limits showed in SS5, using a 850 nm excitation at 46 mJ/cm^2. The absorption spectrum is depicted in turquoise and is vertically shifted for clarity. (c)−(e) TEM images of S2 sample after each synthesis step: PbSe core growth, cation exchange, and SILAR growth of CdS. The scale bar represents 10 nm.

absorbed visible photon. Notably, this ratio improves by nearly a factor of 2 at excitation intensities well above I_{sat}, because under these conditions the system is further excited multiple times following the creation of an exciton (for more details see the supplementary Figure S7). To assess the absolute quantum yield of the upconversion emission as defined above,[26] it is necessary to estimate the visible emission QY, that is, the probability of emission of a visible photon following excitation at 480 nm. For this end, we compare the UC QDs with a reference sample of tellurium doped CdSe/CdS nanorods that emit around 700 nm with 67% QY. Both samples were adjusted to the same OD. at 480 nm and excited at I_{sat}. By integrating the fluorescence emission spectra, we estimated the QY of S1 to be 5%. Thus, the overall UC efficiency of our system can be estimated as $QY_{CdSe(WZ)} \cdot \epsilon_{UC} \sim 5\% \cdot 0.075 - 0.4\%$ at I_{sat}, and up to about 0.7% well above saturation (i.e., for every 150−250 photons absorbed we have one upconverted photon). This efficiency is within the range of efficiencies reported for other types of UC nanoparticles, while exhibiting broadband upconversion in a presently inaccessible spectral range.

The important attributes in using a NC UC system is the ability to extract hot charges at the nanoscale, which can compete with cooling and nonradiative decay processes. Moreover, tunability and versatility can be achieved by changing the original PbSe QD size and the CdSe shell volume, by using these two parameters one can tweak both the visible emission wavelength and the NIR absorption edge. To show this system's versatility and tunability, a second PbSe/CdSe/CdS NCs sample ("S2") was synthesized by starting form a slightly different core size (diameter 7.4). The S2 sample, similarly to S1, exhibits a broad NIR emission around 1260 nm after cation exchange but a visible emission peak at 630 nm (Figure 6b). This result stresses the promise of this system that can easily be tuned, by controlling the initial PbSe core diameter and the CdSe shell volume. The latter is readily achieved by controlling the extent of cation exchange, while

DOI: 10.1021/acsnano.5b05329
ACS Nano XXXX, XXX, XXX−XXX

easily changing the NIR and visible emission peak positions. As depicted in Figure 6a, the fluorescence emission peak at 630 nm shows a quadratic power dependence characteristic of a 2-photon UC process and a fast decay lifetime of 10 ns (Figure SS5, Supporting Information), meaning that a successful UC can be achieved from the NIR to 630 nm. As can be seen in Figure 6b, the visible emission at 630 nm is broadened by another smaller emission peak at 700 nm, likely caused by the presence of two sizes within the sample. This is probably the result of etching and Oswald ripening in the final stage of the synthesis. However, as can be seen in Figure 6b, the upconverted emission spectrum, using 46 mJ/cm^2 850 nm excitation, fits the linear excitation using a 405 nm LED. Moreover, having the second peak does not disrupt the optical measurements, as the emission was spectrally filtered using a monochromator. In doing so, the photophysics of both peaks could be checked separately and were found to be relatively similar, both exhibiting nonlinear 2-photon attributes.

CONCLUSIONS

In conclusion, the synthesis of double emitting QDs which exhibit NIR UC capabilities at room temperature was demonstrated. At saturation, 7 near-infrared photon pairs are equivalent to the absorption of a single visible photon, and a total UC efficiency of 0.4% (up to 0.7% well above saturation) was achieved, comparable to alternative nanocrystalline systems. The synthesis is a three-step process, which enables versatility and tunability of both the visible emission color and the NIR absorption edge, by tweaking the shell volume exchanged and the original core size of PbSe. Using this method, one can achieve a range of desired upconverted emission peak positions with a suitable NIR band gap. This promising attribute of broadband NIR response and band edge tunability is lacking in other methods for UC, such as use of lanthanide-based materials, and triplet triplet annihilation, both of which are restricted due to the limited selection of available lanthanides and molecules. Hence, these NCs can be attractive and promising for use in solar cells that will be able to upconvert the solar NIR spectrum to fit the junction band gap in solid state systems. In particular, for silicon photovoltaic devices, these NCs could be used to surpass the known Shockley–Queisser efficiency limit, by converting NIR photons to fit the silicon 1.1 eV band gap. Moreover, such NCs could be used to convert mid-IR photons to photons in the region detectable by InGaAs detectors (up to 1.7 μm) due to the broad tunability of lead chalcogenide nanocrystals.

Color tunability should be most beneficial for biological imaging, having the ability to synthesize a wide range of PbSe/CdSe/CdS samples, tweaking and choosing the suitable desired excitation wavelength and emission. These NC's could act as labeling dyes for the system requirements maintaining high SNR and low tissue scattering.

Moreover, the application of this system can be extended to different lead chalcogenide core/shell nanocrystals or alloys, providing additional knobs for controlling their optical properties. A more detailed study of the effects of the CdSe and CdS shell thickness on the upconverted emission quantum yield is likely to enable fabrication of even more efficient UC nanocrystals.

METHODS

Synthesis. All syntheses were performed under Ar flow using standard Schlenk techniques. PbSe synthesis and cation exchange were performed according to previous reports with slight modifications.[28,34]

PbSe QDs Synthesis. A 0.892 g sample of PbO was dissolved in 4 mL of OA and 16 mL of ODE by degassing it for 2 h in 120 °C, followed by drying under Ar flow for half an hour. Four milliliters of 2 M TOP-Se was injected at 180 °C while maintaining a growth temperature of 160–170 °C for 1–8 min, depending on the desired size. The reaction was stopped by removing the heating mantle and cooling with a water bath. The PbSe QDs were purified twice in the glovebox, using ethanol as a polar solvent for precipitation.

PbSe/CdSe QD Synthesis. Clean PbSe QDs in toluene were added to a cadmium oleate (Cd-OA) 0.5 M solution, and the mixture was degassed for 30 min in 40 °C to remove the toluene. The cation exchange reaction was performed under Ar flow at 130 °C. The cation exchange reaction time depended on PbSe size and desired CdSe shell thickness. The NCs were purified twice using ethanol for precipitation and redispersed in toluene.

PbSe/CdSe/CdS Synthesis. A CdS shell was grown layer by layer using successive ion adsorption and reaction (SILAR method).[32]

Detailed synthesis procedures are described in the Supporting Information.

TEM and Optical Characterization. UV–vis absorption spectra were measured using a UV–vis–NIR spectrometer (V-670, JASCO). Fluorescence spectra were measured using a custom-made orthogonal collection setup. The excitation was with a fiber coupled 405 nm LED Light Source (prizmatrix), collecting the fluorescence through a fiber, to measure the fluorescence spectrum using either a USB4000 Ocean Optics spectrometer for visible florescence spectrum or a NIR-quest512 spectrometer for NIR fluorescence. TEM images were recorded at 120 kV, using a CM-120, Philips instruments.

Optical Setup. A diluted solution of PbSe/CdSe/CdS NCs dispersed in hexane was placed in 1 × 1 cm^2 quartz cuvette. The sample was excited by 5 ns pulses at 10 Hz, from an optical parametric oscillator (Ekspla NT342/C/3/UVE), or the residual laser pump at 1064 nm. The laser excitation was focused by 1 m lens, and the fluorescence was collected in the orthogonal direction using a 20× 0.4 NA objective, spectrally filtered using a dielectric filter and a monochromator (Acton SpectraPro2150i), and measured by a photomultiplier (Hamamatsu R10699). The photomultiplier transient output was measured by a 600 MHz digital oscilloscope (LeCroy Wavesurfer 62Xs). Pulse energy was measured by a pyroelectric sensor (PE9-C, Ophir Optronics). Transient spectra were taken in each measurement around the fluorescence peak for a series of excitation powers and subtracted for dark noise. Spectra were calculated by integrating the transient PMT measurements and corrected for the PMT response and the dielectric filter transmission spectrum. The NIR emission lifetime was measured using an InGaAs avalanche photodiode (new focus 1647).

ASSOCIATED CONTENT

Supporting Information

The Supporting Information is available free of charge on the ACS Publications website at DOI: 10.1021/acsnano.5b05329.

Details of synthesis, TEM images, TEM and optical characterization, absorption spectra, a more detailed description of the optical setup, transient curves, and fit of the saturation curves (PDF)

AUTHOR INFORMATION

Corresponding Author

*D. Oron. E-mail: dan.oron@weizmann.ac.il

Notes

The authors declare no competing financial interest.

DOI: 10.1021/acsnano.5b05329
ACS Nano XXXX, XXX, XXX–XXX

ACKNOWLEDGMENTS

This research was supported by a research grant from Dana and Yossie Hollander, by the Israeli Centers of Research Excellence program, by the European Research Council starting investigator grant SINSLIM 258221 and by the Israeli Ministry of Economy Focal Technology Area research grant. A.T. acknowledges support by the ASER fellowship.

REFERENCES

(1) Braun, M.; Burda, C.; El-Sayed, M. a. Variation of the Thickness and Number of Wells in the CdS/HgS/CdS Quantum Dot Quantum Well System. *J. Phys. Chem. A* **2001**, *105*, 5548−5551.
(2) Battaglia, D.; Blackman, B.; Peng, X. Coupled and Decoupled Dual Quantum Systems in One Semiconductor Nanocrystal. *J. Am. Chem. Soc.* **2005**, *127*, 10889−10897.
(3) Dias, E. a.; Grimes, A. F.; English, D. S.; Kambhampati, P. Single Dot Spectroscopy of Two-Color Quantum Dot/quantum Shell Nanostructures. *J. Phys. Chem. C* **2008**, *112*, 14229−14232.
(4) Dias, E. a.; Saari, J. I.; Tyagi, P.; Kambhampati, P. Improving Optical Gain Performance in Semiconductor Quantum Dots *via* Coupled Quantum Shells. *J. Phys. Chem. C* **2012**, *116*, 5407−5413.
(5) Tyagi, P.; Kambhampati, P. Independent Control of Electron and Hole Localization in Core/ Barrier/Shell Nanostructures. *J. Phys. Chem. C* **2012**, *116*, 8154−8160.
(6) Soni, U.; Pal, A.; Singh, S.; Mittal, M.; Yadav, S.; Elangovan, R.; Sapra, S. Simultaneous Type-I/Type-II Emission from CdSe/CdS/ZnSe Nano-Heterostructures. *ACS Nano* **2014**, *8*, 113−123.
(7) Htoon, H.; Malko, a. V.; Bussian, D.; Vela, J.; Chen, Y.; Hollingsworth, J. a.; Klimov, V. I. Highly Emissive Multiexcitons in Steady-State Photoluminescence of Individual "Giant" CdSe/CdS Core/Shell Nanocrystals. *Nano Lett.* **2010**, *10*, 2401−2407.
(8) Kundu, J.; Ghosh, Y.; Dennis, A. M.; Htoon, H.; Hollingsworth, J. a. Giant Nanocrystal Quantum Dots: Stable down-Conversion Phosphors That Exploit a Large Stokes Shift and Efficient Shell-to-Core Energy Relaxation. *Nano Lett.* **2012**, *12*, 3031−3037.
(9) Lutich, A. a.; Mauser, C.; Da Como, E.; Huang, J.; Vaneski, A.; Talapin, D. V.; Rogach, A. L.; Feldmann, J. Multiexcitonic Dual Emission in CdSe/CdS Tetrapods and Nanorods. *Nano Lett.* **2010**, *10*, 4646−4650.
(10) Shafran, E.; Borys, N. J.; Huang, J.; Talapin, D. V.; Lupton, J. M. Indirect Exciton Formation due to Inhibited Carrier Thermalization in Single CdSe/CdS Nanocrystals. *J. Phys. Chem. Lett.* **2013**, *4*, 691−697.
(11) Wu, W.; Li, M.; Lian, J.; Wu, X.; Yeow, E. K. L.; Jhon, M. H.; Chan, Y. Efficient Color-Tunable Multiexcitonic Dual Wavelength Emission from Type II Semiconductor Tetrapods. *ACS Nano* **2014**, *8*, 9349−9357.
(12) Deutsch, Z.; Schwartz, O.; Tenne, R.; Popovitz-Biro, R.; Oron, D. Two-Color Antibunching from Band-Gap Engineered Colloidal Semiconductor Nanocrystals. *Nano Lett.* **2012**, *12*, 2948−2952.
(13) Deutsch, Z.; Neeman, L.; Oron, D. Luminescence Upconversion in Colloidal Double Quantum Dots. *Nat. Nanotechnol.* **2013**, *8*, 649−653.
(14) Haase, M.; Schäfer, H. Upconverting Nanoparticles. *Angew. Chem., Int. Ed.* **2011**, *50*, 5808−5829.
(15) Auzel, F. Upconversion and Anti-Stokes Processes with F and D Ions in Solids. *Chem. Rev.* **2004**, *104*, 139−173.
(16) Trupke, T.; Green, M. a.; Würfel, P. Improving Solar Cell Efficiencies by up-Conversion of Sub-Band-Gap Light. *J. Appl. Phys.* **2002**, *92*, 4117.
(17) Zhou, J.; Liu, Z.; Li, F. Upconversion Nanophosphors for Small-Animal Imaging. *Chem. Soc. Rev.* **2012**, *41*, 1323−1349.
(18) Shockley, W.; Queisser, H. J. Detailed Balance Limit of Efficiency of P-N Junction Solar Cells. *J. Appl. Phys.* **1961**, *32*, 510.
(19) Wu, S.; Han, G.; Milliron, D. J.; Aloni, S.; Altoe, V.; Talapin, D. V.; Cohen, B. E.; Schuck, P. J. Non-Blinking and Photostable Upconverted Luminescence from Single Lanthanide-Doped Nanocrystals. *Proc. Natl. Acad. Sci. U. S. A.* **2009**, *106*, 10917−10921.
(20) Chan, E. M.; Han, G.; Goldberg, J. D.; Gargas, D. J.; Ostrowski, A. D.; Schuck, P. J.; Cohen, B. E.; Milliron, D. J. Combinatorial Discovery of Lanthanide-Doped Nanocrystals with Spectrally Pure Upconverted Emission. *Nano Lett.* **2012**, *12*, 3839−3845.
(21) Zou, W.; Visser, C.; Maduro, J. Broadband Dye-Sensitized Upconversion of near-Infrared Light. *Nat. Photonics* **2012**, *6*, 560−564.
(22) Parker, C. A.; Hatchard, C. G. Sensitised Anti-Stokes Delayed Fluorescence. *Proceeedings Chem. socity* **1962**, 386−387.
(23) Baluschev, S.; Miteva, T.; Yakutkin, V.; Nelles, G.; Yasuda, a.; Wegner, G. Up-Conversion Fluorescence: Noncoherent Excitation by Sunlight. *Phys. Rev. Lett.* **2006**, *97*, 143903.
(24) Cheng, Y. Y.; Fückel, B.; MacQueen, R. W.; Khoury, T.; Clady, R. G. C. R.; Schulze, T. F.; Ekins-Daukes, N. J.; Crossley, M. J.; Stannowski, B.; Lips, K.; et al. Improving the Light-Harvesting of Amorphous Silicon Solar Cells with Photochemical Upconversion. *Energy Environ. Sci.* **2012**, *5*, 6953.
(25) Singh-Rachford, T. N.; Castellano, F. N. Photon Upconversion Based on Sensitized Triplet−triplet Annihilation. *Coord. Chem. Rev.* **2010**, *254*, 2560−2573.
(26) Boyer, J.-C.; van Veggel, F. C. J. M. Absolute Quantum Yield Measurements of Colloidal NaYF4: Er3+, Yb3+ Upconverting Nanoparticles. *Nanoscale* **2010**, *2*, 1417−1419.
(27) Lin, Q.; Makarov, N. S.; Koh, W.; Velizhanin, K. A.; Cirloganu, C. M.; Luo, H.; Klimov, V. I.; Pietryga, J. M. Design and Synthesis of Heterostructured Quantum Dots with Dual Emission in the Visible and Infrared. *ACS Nano* **2015**, *9*, 539−547.
(28) Cirloganu, C. M.; Padilha, L. a; Lin, Q.; Makarov, N. S.; Velizhanin, K. a; Luo, H.; Robel, I.; Pietryga, J. M.; Klimov, V. I. Enhanced Carrier Multiplication in Engineered Quasi-Type-II Quantum Dots. *Nat. Commun.* **2014**, *5*, 4148.
(29) Zhao, H.; Vomiero, A.; Rosei, F. Ultrasensitive, Biocompatible, Self-Calibrating, Multiparametric Temperature Sensors. *Small* **2015**, *11*, 5741−5746.
(30) Wei, S.; Zhang, S. ZB/WZ Band Offsets and Carrier Localization in CdTe Solar Cells. *NCPV* **2000**, 293−294.
(31) Murayama, M.; Nakayama, T. Chemical Trend of Band Offsets at Wurtzite/zinc-Blende Heterocrystalline Semiconductor Interfaces. *Phys. Rev. B: Condens. Matter Mater. Phys.* **1994**, *49*, 4710−4724.
(32) Li, J. J.; Wang, Y. A.; Guo, W.; Keay, J. C.; Mishima, T. D.; Johnson, M. B.; Peng, X. Large-Scale Synthesis of Nearly Monodisperse CdSe/CdS Core/shell Nanocrystals Using Air-Stable Reagents *via* Successive Ion Layer Adsorption and Reaction. *J. Am. Chem. Soc.* **2003**, *125*, 12567−12575.
(33) Klimov, V. I. Multicarrier Interactions in Semiconductor Nanocrystals in Relation to the Phenomena of Auger Recombination and Carrier Multiplication. *Annu. Rev. Condens. Matter Phys.* **2014**, *5*, 285−316.
(34) Yu, W. W.; Falkner, J. C.; Shih, B. S.; Colvin, V. L. Preparation and Characterization of Monodisperse PbSe Semiconductor Nanocrystals in a Noncoordinating Solvent. *Chem. Mater.* **2004**, *16*, 3318−3322.

DOI: 10.1021/acsnano.5b05329
ACS Nano XXXX, XXX, XXX−XXX